Editors' Suggestion

Self-Trapped Polarons and Topological Defects in a Topological Mott Insulator

Sergi Julià-Farré[1,*] Markus Müller[2,3] Maciej Lewenstein[1,4] and Alexandre Dauphin[1,†]

[1]*ICFO-Institut de Ciencies Fotoniques, The Barcelona Institute of Science and Technology,*
Avinguda Carl Friedrich Gauss 3, 08860 Castelldefels (Barcelona), Spain
[2]*Institute for Quantum Information, RWTH Aachen University, D-52074 Aachen, Germany*
[3]*Peter Grünberg Institute, Theoretical Nanoelectronics, Forschungszentrum Jülich, D-52428 Jülich, Germany*
[4]*ICREA, Passeig Lluís Companys 23, 08010 Barcelona, Spain*

Many-body interactions in topological quantum systems can give rise to new phases of matter, which simultaneously exhibit both rich spatial features and topological properties. In this work, we consider spinless fermions on a checkerboard lattice with nearest and next-to-nearest neighbor interactions. We calculate the phase diagram at half filling, which presents, in particular, an interaction-induced quantum anomalous Hall phase. We study the system at incommensurate fillings using an unrestricted Hartree-Fock ansatz and report a rich zoo of solutions such as self-trapped polarons and domain walls above an interaction-induced topological insulator. We find that, as a consequence of the interplay between the interaction-induced topology and topological defects, these domain walls separate two phases with opposite topological invariants and host topologically protected chiral edge states. Finally, we discuss experimental prospects to observe these novel phenomena in a quantum simulator based on laser-dressed Rydberg atoms in an optical lattice.

Introduction.—First proposed by Feynman in the 1980s [1], quantum simulators are now a reality. These versatile platforms allow for the simulation of complex quantum many-body systems in a clean and highly controllable environment [2]. In particular, cold atoms in optical lattices, with the dramatic advances in atomic, molecular, and optical physics, are highly suitable quantum simulators of many-particle or spin systems with controlled interactions [3]. There, the study of topological insulators with quantum simulators has become a subject of intense research within the past decade [4,5]. These exotic materials constitute a new paradigm of quantum matter [6]: they are characterized by a global order parameter, an integer called topological invariant, and present topologically protected surface currents. The quantum simulation of such phases typically relies on the generation of artificial gauge fields through Floquet engineering [7–10] or synthetic dimensions [11–13].

Recent studies focused on the interplay between external gauge fields and interactions [14–17]. More strikingly, it has been shown that it is also possible to induce topology directly from interactions, hence giving rise to a spontaneous symmetry-breaking (SSB) topological phase [18]. For example, interactions of the same order of magnitude between nearest neighbors (NN) and next-to-nearest neighbors (NNN) give rise to the celebrated topological Mott insulator (TMI) [19,20], an anomalous quantum Hall (QAH) phase [21], in diverse geometries, such as hexagonal, Lieb, checkerboard, and kagome lattices [19,22–30]. To observe

these phases, control over the ratio of interaction strengths is crucial, and cold atoms constitute a prime candidate to simulate such phases in experiment [22,23].

In this Letter, we explore the exotic nature of self-consistent solutions, such as polarons and topological defects, above the TMI. Remarkably, these solutions appear thanks to the interplay of the global topological order and the SSB local order parameter, and are thus absent in gauge-induced topological insulators. In a SSB lattice material, incommensurate fillings can favor static solutions breaking the translational symmetry [31–33]. These solutions, which can also be created in a dynamical way [34–39], can take the form of small perturbations, or topological defects in the local order parameter. In the TMI phase, we are interested in studying the impact of these inhomogeneities on the global topology of the system, and vice versa. In order to shed light onto this question, we abandon the usual assumption of spatially homogeneous TMI phases [19,22–30] and report two type of solutions: (i) self-trapped polarons on top of the topological background and (ii) domain walls between regions from a different sector of the SSB phase. Interestingly, these lead to opposite topological invariants in the same material, and topologically protected chiral edge states at the domain boundaries.

We start by quantitatively studying the Hartree-Fock (HF) phase diagram of a checkerboard lattice of spinless fermions with NN and NNN interactions at half filling. Such phase diagram is in qualitative agreement with the
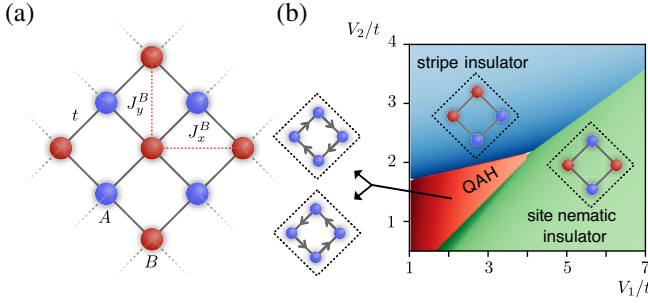
(a)

(b)

FIG. 1. (a) The system is described by a Hamiltonian of spinless fermions $\hat{H}$ on a checkerboard lattice, which has NN and NNN hoppings and interactions. (b) Mean-field phase diagram of the system at half filling in terms of the NN (V_1) and NNN (V_2) interactions. Each SSB phase is represented with a schematic in the four-sites unit-cell ansatz. For the QAH phase, the two degenerate SSB solutions are explicitly shown.

ones obtained with density matrix renormalization group methods [24,26]. We then study the ground state (GS) around half filling in the QAH phase, with an unrestricted Hartree-Fock (UHF) ansatz. The latter is motivated by previous studies in strongly correlated materials, in which UHF methods describe the main physics of the doped GS, up to corrections in the local quantities [40–44]. At low particle doping, we observe a self-trapped polaron and study its effect on the background topological SSB phase. We also analyze the accuracy of the HF method and the interaction between two polarons. For higher fillings, we report the appearance of topological defects in the form of domain walls separating the two sectors of the SSB phase at half filling and inspect the topological chiral edge states on top of them. Finally, we discuss prospects of realizing such phases with cold Rydberg-dressed atoms in optical lattices.

Model.—We consider a Hamiltonian of spinless fermions on a checkerboard lattice with periodic boundary conditions, depicted in Fig. 1(a), $\hat{H} = \hat{H}_0 + \hat{H}_{\text{int}}$, where $\hat{H}_0$ is the quadratic part and $\hat{H}_{\text{int}}$ contains the interactions. On the one hand, the quadratic part of the fermionic Hamiltonian [24–26] reads ($\hbar = 1$)

$$\hat{H}_0 = -t \sum_{\langle ij \rangle} (\hat{c}_{i,A}^\dagger \hat{c}_{j,B} + \text{H.c.})$$
$$+ \sum_i \sum_{\substack{\alpha=A,B \\ \eta=x,y}} (J_\eta^\alpha \hat{c}_{i,\alpha}^\dagger \hat{c}_{i+2\eta,\alpha} + \text{H.c.}) - \mu \sum_i \hat{n}_i, \quad (1)$$

where t stands for the NN hopping amplitude between sites A and B, J_η^α is the NNN hopping amplitude, with $\eta = x, y$ and $\alpha = A, B$, and μ is the chemical potential that controls the fermionic filling. In the remainder of the Letter, we also set $t = 1$, and $J_x^A = J_y^B = +0.5$ and $J_y^A = J_x^B = -0.5$, which generates a π flux on each sublattice. Such Hamiltonian has two bands with a quadratic band touching at half filling. On the other hand, the interaction part of the Hamiltonian reads

$$\hat{H}_{\text{int}} = V_1 \sum_{\langle ij \rangle} \hat{n}_{i,A} \hat{n}_{j,B} + V_2 \sum_{\langle\langle ij \rangle\rangle} \hat{n}_i \hat{n}_j \quad (2)$$

and has NN and NNN density-density repulsive interactions. Such Hamiltonian has a rich phase diagram in terms of V_1/t and V_2/t already at the mean-field level, as will be discussed below.

Phase diagram at half filling.—We treat the interaction Hamiltonian with a standard HF decoupling, respecting the Wick's theorem,

$$\hat{n}_i \hat{n}_j \simeq \bar{n}_i \hat{n}_j + \bar{n}_j \hat{n}_i - \bar{n}_i \bar{n}_j - \xi_{ij} \hat{c}_j^\dagger \hat{c}_i - \xi_{ij}^* \hat{c}_i^\dagger \hat{c}_j + |\xi_{ij}|^2, \quad (3)$$

with $\xi_{ij} = \langle \hat{c}_i^\dagger \hat{c}_j \rangle$ and $\bar{n}_i \equiv \langle \hat{n}_i \rangle$. The HF values ξ_{ij} and $\bar{n}_i$ are found by determining the self-consistent eigenstates λ and energies E of the HF Hamiltonian at zero temperature. We also work with a four-site unit-cell translationally invariant ansatz [see Fig. 1(b)], which we will refer to as the restricted Hartree-Fock (RHF) ansatz in the remainder of the Letter (see Supplemental Material [45]). The phase diagram, presented in Fig. 1(b), has three insulating phases, each of them with an order parameter that captures a broken symmetry: (i) the site nematic insulating phase characterized by $\rho_n \equiv |\bar{n}_{A_1} + \bar{n}_{A_2} - \bar{n}_{B_1} - \bar{n}_{B_2}|$, (ii) the stripe insulating phase, with $\rho_s \equiv |\bar{n}_{A_1} - \bar{n}_{A_2}| + |\bar{n}_{B_1} - \bar{n}_{B_2}|$, and (iii) a QAH phase, with time-reversal symmetry breaking (TRSB) due to interaction-induced closed loops of imaginary NN hopping $\xi_{\text{QAH}} \equiv |\text{Im}(\xi_{A_1 B_1} + \xi_{B_1 A_2} + \xi_{A_2 B_2} + \xi_{B_2 A_1})|/4$. In order to characterize the topology of the QAH phase, we obtain its RHF band structure, which shows two lower filled bands separated from the two upper bands by an energy gap $\Delta_{\text{QAH}} = 8 V_1 \xi_{\text{QAH}}$. We compute the total Chern number ν of the filled bands and find $\nu = \pm 1$ [45]. The two possible values of ν account for the twofold ground-state degeneracy in the interaction-induced QAH phase, i.e., the current loops can flow in two opposite directions, and the system reaches one of the two symmetry-breaking sectors through a spontaneous TRSB mechanism [see Fig. 1(b)].

Self-trapped polaron.—We now focus on the system at low particle doping δ, starting for the case of one extra particle ($\delta = 1$). In the noninteracting rigid band picture, the bulk of the system would lose its insulating character, as the particle would occupy the first single-particle state above the gap. In order to analyze the interacting system, hereafter we fix the value of the interactions to $V_1/t = 2.5$ and $V_2/t = 1.5$. We first study the solution of the RHF ansatz, shown in Fig. 2(a). The self-consistent band structure exhibits only a slight deformation of the bands due to interactions and, indeed, we observe the occupation of a single-particle state above the gap. However, there is also the possibility of lowering the energy by creating states inside the gap, which need to be localized in a finite region of the lattice. In order to capture this scenario, we go one step further and work without the requirement of spatial
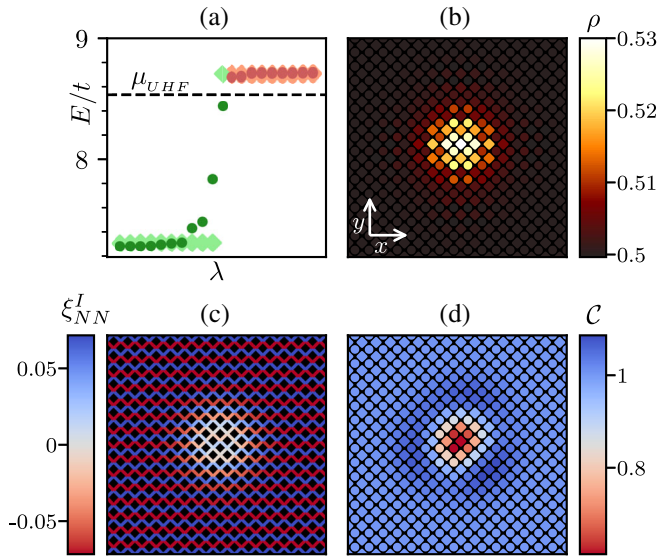
FIG. 2. Self-trapped polaron for $\delta = 1$. (a) Energies of the eigenstates λ around the energy gap for the RHF (diamonds) and UHF (dots) ansatz. The dashed line indicates the chemical potential of the UHF solution, and green (red) colors are used for occupied (empty) states. (b)–(d) Real-space quantities in a region of 16×16 unit cells. (b) Density profile. (c) Imaginary NN hopping $\mathrm{Im}\xi_{i,i+x\pm y}$. (d) Local Chern number.

translational invariance of the HF parameters $(\xi_{ij}, \bar{n}_i)$, known as the UHF ansatz [46,47], on a 24×24 unit-cell lattice. The results are shown in Fig. 2(a): the UHF bands are deformed in order to accommodate the extra particle, with the appearance of states inside the insulating gap, and a decrease of the energy $\Delta E_{\mathrm{UHF}} \equiv \langle H \rangle_{\mathrm{UHF}} - \langle H \rangle_{\mathrm{RHF}} = -0.12t$. These midgap states are localized in a finite region of the lattice, leading to the density cloud shown in Fig. 2(b). We denote such state as the self-trapped polaron solution, as the added particle is confined due to its interaction with the topological background. Notice that this notion of a self-trapped polaron differs from the concept of a mobile polaron quasiparticle in a topological background [48]. Indeed, in this work we focus only on static properties, as it is not warranted that a study of the polaron mobility can be made within a coherent quasiparticle picture due to the interaction-induced localization.

The appearance of self-trapped polarons and other localized excitations has been extensively studied using the UHF method [31–33] for nontopological phases. We here show that the topological character of the material leads to very interesting physics. On the one hand, Fig. 2(c) shows that, in the polaron region, there is a large reduction of the order parameter ξ_{QAH}, accompanied by a change of the SSB sector in the inner region [45]. Notice that this behavior is similar to the one exhibited by the self-trapped antiferromagnetic polaron observed in the 2D Fermi-Hubbard model [31], and can be understood as a collapsed domain wall. On the other hand, and despite the lack of translational invariance, one can characterize the

topology of the system, by means of the local Chern number $\mathcal{C}$ [49–51]. The latter is a real-space quantity that exhibits the same integer quantization as the Chern number ν within the bulk of the material [45]. As shown in Fig. 2(d), this quantity is not quantized at all inside the polaron; however, it stabilizes to $\mathcal{C} = +1$ further away from the latter. We emphasize that, as in the half-filling case, the sign of $\mathcal{C}$ depends on the ground-state SSB sector. Notice also that these local fluctuations of $\mathcal{C}$, which are caused by a spontaneous breaking of translational symmetry, are reminiscent of those induced by quenched disorder in a gauge-induced Chern insulator [52].

Configuration interaction analysis.—We use the configuration interaction method [33,53–55] to analyze the stability of the polaron localization within the UHF ansatz. That is, for different initial conditions on the UHF parameters, we get degenerate polarons centered at different sites, and it is important to check that such localization is not an artifact of the method. In a nutshell, in the configuration interaction method, one lowers the UHF energy by hybridizing several UHF solutions to restore some of the lattice symmetries spontaneously broken in each UHF solution. In our case, we restore the translational invariance of the polaron solution in smaller checkerboard lattices with up to $2 \times 9 \times 9$ sites [45]. Our analysis yields a polaron band supporting the validity of our UHF treatment: the minimum energy of the band is similar to the UHF energy (with a reduction of $\simeq 0.1\%$), and this energy corresponds to a plateau of degenerate states in a region of the band of size $|\Delta \mathbf{k}|$. The latter is compatible with a polaron extended over a finite region with radius $\ell_p \simeq 1/|\Delta \mathbf{k}|$, as observed in the UHF solution.

Two polarons.—For two extra particles ($\delta = 2$) we find two types of self-consistent solutions. The lowest energy solution is a composite state of two polarons [see Fig. 3(a)]. The inner region of this bipolaron, slightly larger than the one corresponding to the single polaron, also exhibits a change in the SSB sector [45]. The other type of solutions corresponds to two spatially nonoverlapping polarons [see Fig. 3(b)]. The latter are metastable solutions with a higher energy than the composite state, which indicates that there is an attractive interaction between polarons. However, for large initial separations, individual polarons are likely to be detectable. In order to characterize the formation of these metastable solutions, we choose for the initial UHF values those of a spatial superposition of two single polarons, and vary their initial separation. Figure 3(c) shows the final distance between them d_{p-p} as a function of their initial separation d_{p-p}^0. Considering the self-consistent UHF algorithm as some virtual dynamics for the HF parameters, we observe a collapse radius $d_{p-p}^0 \simeq 12$ in the initial separation, below which the two polarons interact until the stabilization of the lowest energy composite solution with $d_{p-p} \simeq 9$. At larger initial separations, the system
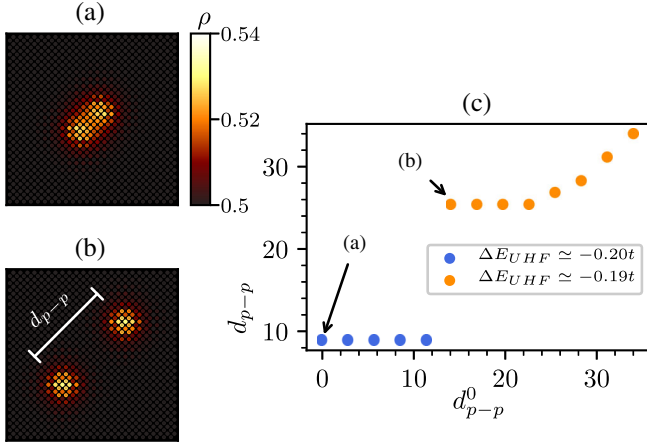
FIG. 3. Two polarons for $\delta = 2$. (a),(b) Density profile of the composite and nonoverlapping solutions. (c) Final distance between the two polarons, taken as the separation between the two sites with largest density, as a function of the separation in the initial ansatz for the UHF values. Blue (orange) circles correspond to composite (nonoverlapping) solutions.

stabilizes the nonoverlapping solution, with a forbidden range $d_{p-p} \in (12, 25]$, showing that metastable solutions avoid residual overlaps.

Ring-shaped domain walls.—Even at higher particle doping, we find that the system retains its bulk insulating character: it is energetically favorable to create several midgap localized states, as can be seen in Fig. 4(a) for $\delta = 8$. Taking as a reference the polaron solutions, the attractive interaction between them leads to a GS whose inner region is in the other SSB sector [45]. For a sufficiently large value of δ, this eventually leads to the formation of a domain wall between two extended half-filling regions that are in the QAH phase, as can be seen in Fig. 4(b). Interestingly, the inversion of the TRSB order parameter across the domain wall leads to the two opposite values of the local Chern number $\mathcal{C} = \pm 1$ depicted in Fig. 4(b). Notice here the role of interactions, leading to a SSB: the coexistence of topologically opposite phases would not occur if the Chern insulator was induced by a homogeneous external gauge field, that would define the global topology sector of the system. Furthermore, the change of the local Chern number $|\Delta\mathcal{C}| = 2$ between the two regions gives rise to topologically protected edge states with a fixed chirality in the ring. This is exactly what we observe in the GS currents $\mathcal{J}_{x(y)} \equiv 2J_{x(y)}^{A/B}\text{Im}\langle\hat{c}_{i+x(y)}^{\dagger}\hat{c}_i\rangle$ shown in Figs. 4(c) and 4(d), which are carried by midgap states. We also verified that the solution with $\mathcal{C} = -1$ in the inner part of the ring and $\mathcal{C} = 1$ in the outer part has the same energy and presents edge states with opposite chirality [45].

Linear domain walls.—For $\delta = 8$, we also find a metastable self-consistent solution, in which the system develops two domain walls (see Fig. 5). The extra density is deposited in these linear structures, as depicted in Fig. 5(b).
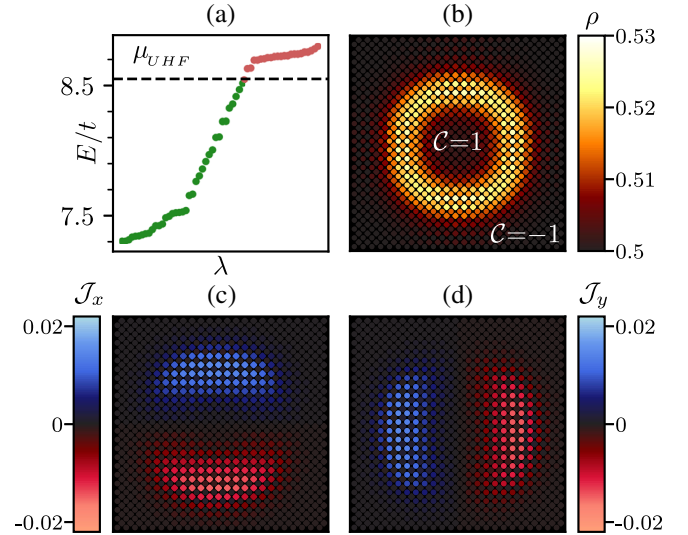

FIG. 4. Domain wall for $\delta = 8$. This UHF solution lowers the RHF energy by $\Delta E_{\text{UHF}} \simeq -0.67t$. (a) Single-particle energies in the gap region. (b) Density profile. Here we indicate the approximately constant value of $\mathcal{C}$ in the inner and outer regions of the ring. (c),(d) GS currents $\mathcal{J}_x$ and $\mathcal{J}_y$.

As in the previous case, the domain walls separate two regions with a reversed TRSB order parameter, leading to two opposite values of the local Chern number, as can be seen in Fig. 5(c). The main difference, however, is that here the change in the local Chern number $|\Delta\mathcal{C}| = 2$ occurs in each of the two disconnected domain walls, leading to pairs
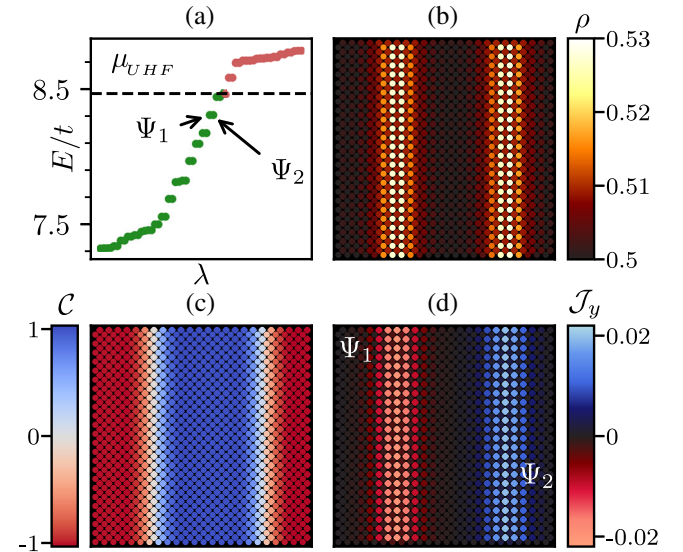

FIG. 5. Linear domain walls for $\delta = 8$. This metastable UHF solution lowers the RHF energy by $\Delta E_{\text{UHF}} \simeq -0.65t$. (a) Energies in the gap region, with two degenerate edge states Ψ_1 and Ψ_2. (b) Density profile. (c) Local Chern number. (d) Current $\mathcal{J}_y$ flowing in opposite directions at each boundary, and carried by midgap states such as Ψ_1 and Ψ_2.

of degenerate chiral edge states (one at each domain wall) with opposite chiralities, as shown in Figs. 5(a)–5(d).

Quantum simulation with Rydberg atoms in an optical lattice.—Cold atoms in optical lattices provide a prime candidate platform to implement the interacting fermionic Hamiltonian $\hat{H}$ and observe the interaction-induced polarons and topological defects in a highly controllable experimental setup (for further details, see Ref. [45]): Laser coupling between different sublattices (cf. Fig. 1), similar to the approach taken in Ref. [56], allows one to control hopping dynamics as described by Eq. (1). Optically trapped and laser-excited Rydberg atoms have become a versatile platform for quantum simulation of many-body physics [57–59]. Weak off-resonant laser dressing of GS atoms with Rydberg states, as demonstrated, e.g., in Ref. [60] allows one to induce effective NN and NNN interactions, with associated energy scale V_2 of a similar magnitude as V_1 [22,23,61–63], and both compatible with the kinetic energy scales of Eq. (1). Detrimental incoherent processes, such as dephasing and radiative decay from metastable Rydberg states, are small for suitably chosen laser and atomic parameters [64] and occur at timescales larger than those associated to the effective couplings of Hamiltonian (2) governing the coherent system dynamics. For $t \sim 1$ kHz, temperatures $T \lesssim 10$ nK are below the critical temperature of the QAH phase and the typical decrease in energy due to the appearance of spatial structures inside the bulk gap. In addition, techniques specifically adapted to the detection of the Chern number, such as time of flight [56,65], transport [8,66], or interband transition [9,67] measurements or the detection of edge states on the domain walls through real-space-density imaging [56,68], could be generalized to resolve the predicted interaction-induced polarons and topological defects.

[*] sergi.julia@icfo.eu
[†] alexandre.dauphin@icfo.eu

[1] R. P. Feynman, Int. J. Theor. Phys. **21,** 467 (1982).
[2] M. Lewenstein, A. Sanpera, and V. Ahufinger, *Ultracold Atoms in Optical Lattices: Simulating Quantum Many Body Systems*, 2nd ed. (Oxford University Press, Oxford, 2017).
[3] I. Bloch, J. Dalibard, and W. Zwerger, Rev. Mod. Phys. **80,** 885 (2008).
[4] N. Goldman, G. Juzeliūnas, P. Öhberg, and I. B. Spielman, Rep. Prog. Phys. **77,** 126401 (2014).
[5] N. R. Cooper, J. Dalibard, and I. B. Spielman, Rev. Mod. Phys. **91,** 015005 (2019).
[6] M. Z. Hasan and C. L. Kane, Rev. Mod. Phys. **82,** 3045 (2010).
[7] H. Miyake, G. A. Siviloglou, C. J. Kennedy, W. C. Burton, and W. Ketterle, Phys. Rev. Lett. **111,** 185302 (2013).
[8] M. Aidelsburger, M. Lohse, C. Schweizer, M. Atala, J. T. Barreiro, S. Nascimbène, N. R. Cooper, I. Bloch, and N. Goldman, Nat. Phys. **11,** 162 (2015).
[9] L. Asteria, D. T. Tran, T. Ozawa, M. Tarnowski, B. S. Rem, N. Fläschner, K. Sengstock, N. Goldman, and C. Weitenberg, Nat. Phys. **15,** 449 (2019).
[10] G. Jotzu, M. Messer, R. Desbuquois, M. Lebrat, T. Uehlinger, D. Greif, and T. Esslinger, Nature (London) **515,** 237 (2014).
[11] A. Celi, P. Massignan, J. Ruseckas, N. Goldman, I. B. Spielman, G. Juzeliūnas, and M. Lewenstein, Phys. Rev. Lett. **112,** 043001 (2014).
[12] B. K. Stuhl, H.-I. Lu, L. M. Aycock, D. Genkina, and I. B. Spielman, Science **349,** 1514 (2015).
[13] M. Mancini, G. Pagano, G. Cappellini, L. Livi, M. Rider, J. Catani, C. Sias, P. Zoller, M. Inguscio, M. Dalmonte, and L. Fallani, Science **349,** 1510 (2015).
[14] S. Rachel and K. Le Hur, Phys. Rev. B **82,** 075106 (2010).
[15] C. N. Varney, K. Sun, M. Rigol, and V. Galitski, Phys. Rev. B **82,** 115125 (2010).
[16] T. I. Vanhala, T. Siro, L. Liang, M. Troyer, A. Harju, and P. Törmä, Phys. Rev. Lett. **116,** 225305 (2016).
[17] I. S. Tupitsyn and N. V. Prokof'ev, Phys. Rev. B **99,** 121113 (R) (2019).
[18] S. Rachel, Rep. Prog. Phys. **81,** 116501 (2018).
[19] S. Raghu, X.-L. Qi, C. Honerkamp, and S.-C. Zhang, Phys. Rev. Lett. **100,** 156401 (2008).
[20] K. Sun and E. Fradkin, Phys. Rev. B **78,** 245122 (2008).
[21] F. D. M. Haldane, Phys. Rev. Lett. **61,** 2015 (1988).
[22] A. Dauphin, M. Müller, and M. A. Martin-Delgado, Phys. Rev. A **86,** 053618 (2012).
[23] A. Dauphin, M. Müller, and M. A. Martin-Delgado, Phys. Rev. A **93,** 043611 (2016).
[24] T.-S. Zeng, W. Zhu, and D. Sheng, npj Quantum Mater. **3,** 49 (2018).
[25] K. Sun, H. Yao, E. Fradkin, and S. A. Kivelson, Phys. Rev. Lett. **103,** 046811 (2009).
[26] S. Sur, S.-S. Gong, K. Yang, and O. Vafek, Phys. Rev. B **98,** 125144 (2018).
[27] H.-Q. Wu, Y.-Y. He, C. Fang, Z. Y. Meng, and Z.-Y. Lu, Phys. Rev. Lett. **117,** 066403 (2016).
[28] E. V. Castro, A. G. Grushin, B. Valenzuela, M. A. H. Vozmediano, A. Cortijo, and F. de Juan, Phys. Rev. Lett. **107,** 106402 (2011).

[29] A. G. Grushin, E. V. Castro, A. Cortijo, F. de Juan, M. A. H. Vozmediano, and B. Valenzuela, Phys. Rev. B **87**, 085136 (2013).

[30] C. Weeks and M. Franz, Phys. Rev. B **82**, 085310 (2010).

[31] J. A. Vergés, E. Louis, P. S. Lomdahl, F. Guinea, and A. R. Bishop, Phys. Rev. B **43**, 6099 (1991).

[32] J. A. Vergés, F. Guinea, and E. Louis, Phys. Rev. B **46**, 3562 (1992).

[33] A. Rüegg and G. A. Fiete, Phys. Rev. B **83**, 165118 (2011).

[34] T. W. B. Kibble, J. Phys. A **9**, 1387 (1976).

[35] W. H. Zurek, Nature (London) **317**, 505 (1985).

[36] A. del Campo and W. H. Zurek, Int. J. Mod. Phys. A **29**, 1430018 (2014).

[37] A. Polkovnikov, Phys. Rev. B **72**, 161201(R) (2005).

[38] W. H. Zurek, U. Dorner, and P. Zoller, Phys. Rev. Lett. **95**, 105701 (2005).

[39] A. Keesling, A. Omran, H. Levine, H. Bernien, H. Pichler, S. Choi, R. Samajdar, S. Schwartz, P. Silvi, S. Sachdev, P. Zoller, M. Endres, M. Greiner, V. Vuletić, and M. D. Lukin, Nature (London) **568**, 207 (2019).

[40] D. Poilblanc and T. M. Rice, Phys. Rev. B **39**, 9749 (1989).

[41] J. Zaanen and O. Gunnarsson, Phys. Rev. B **40**, 7391 (1989).

[42] K. Machida, Physica (Amsterdam) **158C**, 192 (1989).

[43] H. Schulz, J. Phys. (Paris) **50**, 2833 (1989).

[44] B.-X. Zheng, C.-M. Chung, P. Corboz, G. Ehlers, M.-P. Qin, R. M. Noack, H. Shi, S. R. White, S. Zhang, and G. K.-L. Chan, Science **358**, 1155 (2017).

[45] See Supplemental Material at http://link.aps.org/supplemental/10.1103/PhysRevLett.125.240601 for details on the analytical and numerical calculations and an extended discussion of the experimental scheme.

[46] G. W. Pratt, Phys. Rev. **102**, 1303 (1956).

[47] H. Fukutome, Int. J. Quantum Chem. **20**, 955 (1981).

[48] A. Camacho-Guardian, N. Goldman, P. Massignan, and G. M. Bruun, Phys. Rev. B **99**, 081105(R) (2019).

[49] R. Bianco and R. Resta, Phys. Rev. B **84**, 241106(R) (2011).

[50] R. Bianco, Chern invariant and orbital magnetization as local quantities, Ph.D. thesis, Università degli studi di Trieste, 2014.

[51] D.-T. Tran, A. Dauphin, N. Goldman, and P. Gaspard, Phys. Rev. B **91**, 085125 (2015).

[52] L. Ulčakar, J. Mravlje, and T. Rejec, Phys. Rev. Lett. **125**, 216601 (2020).

[53] E. Louis, F. Guinea, M. P. L. Sancho, and J. A. Vergés, Phys. Rev. B **59**, 14005 (1999).

[54] K. Ferhat and A. Ralko, Phys. Rev. B **89**, 155141 (2014).

[55] F. Plasser, M. Ruckenbauer, S. Mai, M. Oppel, P. Marquetand, and L. González, J. Chem. Theory Comput. **12**, 1207 (2016).

[56] N. Goldman, E. Anisimovas, F. Gerbier, P. Öhberg, I. B. Spielman, and G. Juzeliūnas, New J. Phys. **15**, 013025 (2013).

[57] T. F. Gallagher, *Rydberg Atoms*, Cambridge Monographs on Atomic, Molecular and Chemical Physics (Cambridge University Press, Cambridge, England, 1994).

[58] A. Browaeys and T. Lahaye, Nat. Phys. **16**, 132 (2020).

[59] H. Bernien, S. Schwartz, A. Keesling, H. Levine, A. Omran, H. Pichler, S. Choi, A. S. Zibrov, M. Endres, M. Greiner, V. Vuletić, and M. D. Lukin, Nature (London) **551**, 579 (2017).

[60] J. Zeiher, R. van Bijnen, P. Schauß, S. Hild, J.-y. Choi, T. Pohl, I. Bloch, and C. Gross, Nat. Phys. **12**, 1095 (2016).

[61] M. Saffman, T. G. Walker, and K. Mølmer, Rev. Mod. Phys. **82**, 2313 (2010).

[62] N. Henkel, R. Nath, and T. Pohl, Phys. Rev. Lett. **104**, 195302 (2010).

[63] G. Pupillo, A. Micheli, M. Boninsegni, I. Lesanovsky, and P. Zoller, Phys. Rev. Lett. **104**, 223002 (2010).

[64] J. B. Balewski, A. T. Krupp, A. Gaj, S. Hofferberth, R. Löw, and T. Pfau, New J. Phys. **16**, 063012 (2014).

[65] E. Alba, X. Fernandez-Gonzalvo, J. Mur-Petit, J. K. Pachos, and J. J. Garcia-Ripoll, Phys. Rev. Lett. **107**, 235301 (2011).

[66] A. Dauphin and N. Goldman, Phys. Rev. Lett. **111**, 135302 (2013).

[67] D. T. Tran, A. Dauphin, A. G. Grushin, P. Zoller, and N. Goldman, Sci. Adv. **3**, e1701207 (2017).

[68] N. Goldman, G. Jotzu, M. Messer, F. Görg, R. Desbuquois, and T. Esslinger, Phys. Rev. A **94**, 043611 (2016).